Algorithm for the Joint Flight of Two Uncrewed Aerial Vehicles Constituting a Bistatic Radar System for the Soil Remote Sensing

Gennady Linets, Anatoliy Bazhenov, Sergey Malygin, Natalia Grivennaya*, Tatiana Chernysheva and Sergey Melnikov

Department of Infocommunications, North Caucasus Federal University, Pushkin str., 1, Stavropol, 355000, Russia

ABSTRACT

The study of soil agrophysical and agrochemical properties is based on ground-based point measurements and measurements conducted using radiometric remote sensing systems (satellite or airborne). A disadvantage of the existing remote sensing systems using normal surface irradiation is the insignificant depth of penetration of the probing radiation into the soil layer. It is proposed to use a radar system for remote sensing agricultural lands to eliminate this drawback. The system uses a method for assessing the soil's physical and chemical properties based on the interference measurements of direct and reflected electromagnetic waves at incidence angles that provide a total refraction effect, i.e., close to Brewster's angle. The possibility of using this method for remote assessment of soil's physical and chemical properties, including the subsurface layer moisture, was established. A feature of the bistatic system is that it is necessary to coordinate the mutual arrangement of the transmitting and receiving positions, which imposes special requirements on the UAVs' flight algorithm. The UAVs' relative position makes it possible to form the conditions for the manifestation of the total refraction effect, to determine the current value of Brewster's angle, and to fix these conditions for the subsequent flight, making it possible to measure the soil's physical and chemical parameters. The research results can be used to implement precision farming technology in hard-to-reach places, large agricultural areas, and digital agriculture.

Keywords: Brewster's angle, flight algorithm, radar system, remote sensing, soil moisture, total refraction, UAV

INTRODUCTION

Soil moisture (SM) is one of the most important parameters in agricultural applications such as agricultural land mapping (Dari et al., 2021), irrigation planning, flood monitoring (S. Wang et al., 2021), draft monitoring (Filion et al., 2016), and yield forecasting (Brook et al., 2020). They can promote water-saving agriculture (Tran et al., 2015) and provide food security, especially in arid and semi-arid regions (Gago et al., 2015; Martins et al., 2021; Fugazza et al., 2022). Traditionally, SM is studied using ground-based point measurements based on interpolated lines or grids using geophysical methods (Tavakol et al., 2021) (tensiometers, neutron moisture meters, capacitive sensors, thermal impulse sensors, underground radars) (Mallet et al., 2021; Xie et al., 2022), which, despite their relatively high accuracy, have limited spatial representativeness (several square meters maximum) (Brook et al., 2020; Babaeian et al., 2021; Rohil & Mathur, 2022; Rouf et al., 2021). Over the past 50 years, active satellite observations in electromagnetic spectra (L (0.39–1.55 GHz), C (3.9–5.75 GHz) and X (5.75–5.75 GHz) and X (5.75–0.9 GHz), rarely P-band) have been used to study SM and multispectral characteristics of vegetation cover (Bargiel et al., 2013; Su et al., 2014; Ludeno et al., 2018; Li et al., 2021; H. Wang et al., 2021). There are also several algorithms (Nguyen et al., 2022), models (Pandey & Jain, 2022; Yang et al., 2021), and software products (Salam et al., 2019; Kim, 2021; Barca et al., 2021) available for real use (Saddik et al., 2021). However, most of the information about SM obtained using radiometric remote (satellite) sensing systems (ASCAT, AMSR-E, AMSR2, SMAP, SMOS) (Amazirh et al., 2018; Faye et al.,2018; Mandal et al.,2020) are usually surface SM (a few millimeters deep for optical and thermal range) (Barca et al., 2021; Elkharrouba et al., 2022) or near surface SM (a few centimeters deep for X-, C-, or L-frequency microwave sensors) (Bandini et al., 2020; Ivushkin et al., 2021). It is not possible to estimate the moisture content of the root zone.

The use of a bistatic (or multistatic) satellite radar system (GNSS-R) (Rohil & Mathur, 2022) makes it possible to partially solve the sounding depth problem by expanding the observation limits (both in angle and operating frequencies) and introducing new parameters due to signal scattering (Kaasiku et al., 2021). Despite the prospects for reflectometry of global navigation satellite signals (Bhogapurapu et al., 2022), cloud cover, vegetation cover, topography, soil structure, climate, and other factors remain significant limitations of the applicability of all remote (satellite) soil sensing methods with relatively high measurement accuracy (Zhu et al., 2019; Babaeian et al., 2021).

Using crewless aircraft makes it possible to remove significant limitations for remote (satellite) sensing (Tran et al., 2015; Gopaiah et al., 2021). The problem of the limited depth of studies of the soil root zone (Sahaar et al., 2022) can be solved by using a radar-sounding system in the ultrashort wave range (up to 860 MHz). The system registers a signal reflected from soil inhomogeneities and carries information about the physical and

chemical properties of the soil (Babaeian et al., 2021). The joint use of the multispectral cameras installed on the UAV and the radar-sounding system will ensure the necessary spatial and temporal consistency of observations of the soil's physical and chemical properties and the state of the surveyed area vegetation cover.

Thus, the relevance of research is determined by the need to expand information sources used in making management decisions in precision farming through radar sounding of subsurface soil layers.

In radar soil sounding, the reflected signal can be represented as the sum of several constituents: the signal falling directly on the receiving antenna, the reflected signal from the air-surface boundary (air-surface interface), and the reflected signal from the inner ground layers located at the entire penetration depth. Given the problem to be solved, the reflection from the air-surface boundary is not informative and, conversely, worsens the conditions for determining the physico-chemical composition of the subsurface soil layers.

As is known, when a plane electromagnetic wave is incident on the interface between two dielectric media, the fraction of reflected energy is determined by the reflection coefficient R. Thus, the purpose of the research is to create conditions under which the reflection coefficient from the air-surface interface will tend to zero ($R \rightarrow 0$), and the energy of the incident wave will penetrate the soil to form a reflected signal from the inner layers. To satisfy this condition, Bazhenov et al. (2021) propose to use the effect of total refraction, i.e., carry out surface irradiation at Brewster's angle, while the remote radar sensing system should be placed on two crewless aerial vehicles (UAVs) and implemented as bistatic. Chandra & Tanzi (2018) performed mathematical modeling of subsurface layers' radar sounding to search for and rescue people during earthquakes and other global disasters using "oblique" surface irradiation at angles close to Brewster's angles. They determined the key requirements for GPR and research conditions and also confirmed the sufficient energy level of the reflected signal to search for objects with an effective scattering surface of about 1 m^2 to a depth of 10 meters.

The disadvantage of existing approaches is that their implementation requires a priori information about the physical and chemical parameters of the soil, namely its dielectric constant and specific conductivity. In this case, Brewster's angle can be calculated from the known expressions. At the same time, the dielectric constant and specific conductivity of the earth's surface layer is not constant value and depends on the soil composition and structure, the presence of salts, and its moisture content. Therefore, before conducting the soil remote sensing with an emphasis on its inner layers, it is necessary to determine the value of Brewster's angle for the specific conditions of radar sounding.

Thus, the scientific task of the study is to develop an algorithm for the flight of two UAVs that make up a bistatic radar system for soil sounding, which allows, under conditions of a priori uncertainty about the physicochemical parameters of the soil surface, provide

the condition (R → 0), determine the current value of Brewster's angle and subsequently maintain flight parameters that make it possible to irradiate the earth's surface at an angle close to Brewster's angle.

MATERIALS AND METHODS

Determination of the main ways of solving the problem and existing restrictions.

The Brewster's angle is determined from the expression for the reflection coefficient for a vertically polarized electromagnetic wave (Bazhenov et al., 2021) (Equation 1):

$$\dot{R}_V = \frac{\dot{Z}_{C2} \cdot \cos \varphi - \dot{Z}_{C1} \cdot \cos \phi}{\dot{Z}_{C2} \cdot \cos \varphi + \dot{Z}_{C1} \cdot \cos \phi}, \qquad [1]$$

with the reflection coefficient equal to zero.

Here, Z_{C1} is the characteristic resistance of the first medium (air); Z_{C2} is the characteristic resistance of the soil surface layer (in the general case, a complex value); φ is the incidence angle of a plane electromagnetic wave on the interface between two media; ϕ is the angle of refraction.

It follows from Equation 1 that to ensure a zero-reflection coefficient R_v, the following condition must be met (Equation 2):

$$\varphi_B = acos \frac{Z_{C1} \cdot \cos \phi}{Z_{C2}}, \qquad [2]$$

where φ_B is Brewster's angle.

The angle of refraction in Equation 2 is determined under Snell's second law in Equation 3,

$$\frac{n_2}{n_1} = \frac{\sin \varphi}{\sin \phi}, \qquad [3]$$

where n_1, n_2 is the refractive indices of the first and second medium.

Figures 1(a) and 1(b) show the reflection coefficient's dependence on the incidence angle for radio waves with vertical and horizontal polarizations. In Figure 1(a), the specific conductivity of soil is 0.017 S/m, corresponding to dry soil. Figure 1b shows the soil-specific conductivity of 0.7 S/m, i.e., highly moistened soil.

As follows from Figures 1(a) and 1(b), an increase in specific conductivity leads to a shift in Brewster's angle towards larger values, and in this case, the minimum value of the reflection coefficient is increasingly different from zero.

In the absence of a priori data on the specific conductivity and permittivity, it is not possible to determine the value of Brewster's angle only from the amplitude of the radar signal reflected from the earth's surface since the total received signal may not have a pronounced minimum at this angle of incidence.
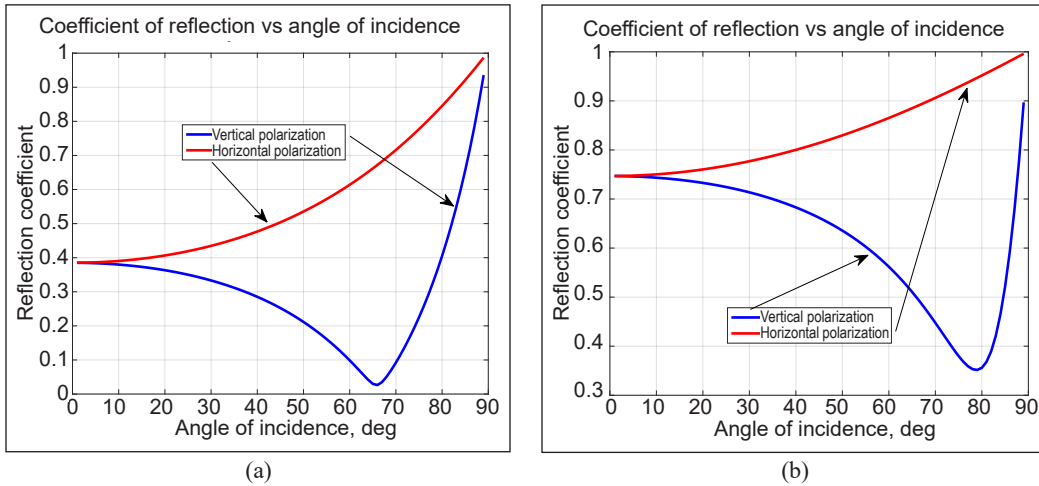
Figure 1. The dependence of the reflection coefficient on the angle of incidence: (a) specific conductivity of soil is 0.017 S/m; (b) specific conductivity of soil is 0.7 S/m

It is proposed to use the interference of direct and reflected waves with the successive application of vertical and horizontal polarization to substantiate the algorithm for the joint flight of two crewless aerial vehicles that make up a bistatic radar system for remote soil sensing, which provides the detection of the total refraction effect. Figure 2 shows the conditions for the formation of the interference wave.

In Figure 2, the following designations are accepted: h_1 and h_2 are the heights of the transmitting and receiving antennas, respectively; φ is the angle of incidence; $L_1 = h_1 \cdot tg\varphi$ is the projection on the Earth's surface of the distance D_1 between the transmitting position and the place where the reflected signal is formed; $L_2 = h_2 \cdot tg\varphi$ is the projection onto the Earth's surface of the distance D_2 between the receiving position and the place where the reflected signal is formed; $L = (h_1 + h_2) \cdot tg\varphi$ is the sum of distances L_1 и L_2; $D_0 = \sqrt{(h_1 - h_2)^2 + L^2}$ is the path that the direct wave travels. In sum, $D_1 = \sqrt{h_1^2 + L_1^2}$ and $D_2 = \sqrt{h_2^2 + L_2^2}$ are the path traveled by the reflected wave.

The instantaneous value of the direct wave amplitude at the moment t has the form presented in Equation 4,

$$U_0 = A \cdot e^{-j\omega t} \cdot e^{-j\frac{2\pi}{\lambda}D_0} \qquad [4]$$

Here, A is the electric field strength; $\omega = 2\pi f$ is the cyclic signal frequency and λ wavelength.
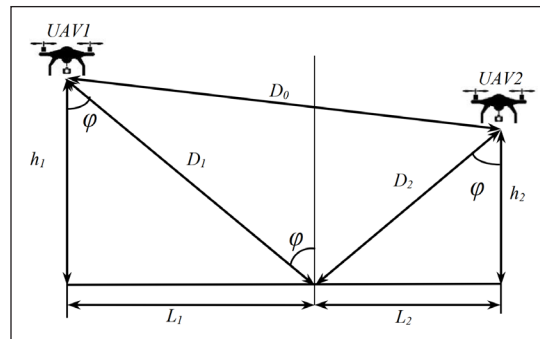

Figure 2. Conditions for the formation of the interference wave

The instantaneous value of the reflected wave amplitude at the moment t is determined by Equation 5:

$$U_1 = A \cdot \dot{R} \cdot e^{-j\omega t} \cdot e^{-j\frac{2\pi}{\lambda}\left(\sqrt{h_1^2+L_1^2}+\sqrt{h_2^2+L_2^2}\right)}. \qquad [5]$$

Considering Equations 4 and 5, the total signal $U_\Sigma = U_0 + U_1$ will be as stated in Equation 6:

$$U_\Sigma = A \cdot e^{-j\omega t} \left(e^{-j\frac{2\pi}{\lambda}D_0} + \dot{R} \cdot e^{-j\frac{2\pi}{\lambda}(D_1+D_2)}\right). \qquad [6]$$

Considering the substitution $\dot{K} = A \cdot e^{-j\omega t}$, Equation 6 can be written as Equation 7:

$$\dot{U}_Z = \dot{K} \cdot \left(e^{-j\frac{2\pi}{\lambda}D_0} + \dot{R} \cdot e^{-j\frac{2\pi}{\lambda}(D_1+D_2)}\right). \qquad [7]$$

The reflection coefficient R˙ for a lossy dielectric such as wet soil will have a complex character and different formulas for calculating vertical and horizontal polarization. Substituting the formula for calculating the reflection coefficient for horizontal polarization into Equation 7, we obtain the expression for the total wave presented in Equation 8:

$$\dot{U}_{ZH} = \dot{K} \cdot \left[\left\{cos\left(\frac{2\pi}{\lambda} \cdot D_0\right) - j \cdot sin\left(\frac{2\pi}{\lambda} \cdot D_0\right)\right\} + \frac{\dot{Z}_{C2} \cdot cos\,\phi - \dot{Z}_{C1} \cdot cos\,\varphi}{\dot{Z}_{C2} \cdot cos\,\phi + \dot{Z}_{C1} \cdot cos\,\varphi} \cdot \right.$$
$$\left. \cdot \left\{cos\left(\frac{2\pi}{\lambda} \cdot (D_1 + D_2)\right) - j \cdot sin\left(\frac{2\pi}{\lambda} \cdot (D_1 + D_2)\right)\right\}\right]. \qquad [8]$$

For vertical polarization, Equation 7 will be as follows, presented as Equation 9:

$$\dot{U}_{ZV} = \dot{K} \cdot \left[\left\{cos\left(\frac{2\pi}{\lambda} \cdot D_0\right) - j \cdot sin\left(\frac{2\pi}{\lambda} \cdot D_0\right)\right\} + \frac{\dot{Z}_{C2} \cdot cos\,\varphi - \dot{Z}_{C1} \cdot cos\,\phi}{\dot{Z}_{C2} \cdot cos\,\varphi + \dot{Z}_{C1} \cdot cos\,\phi} \cdot \right.$$
$$\left. \cdot \left\{cos\left(\frac{2\pi}{\lambda} \cdot (D_1 + D_2)\right) - j \cdot sin\left(\frac{2\pi}{\lambda} \cdot (D_1 + D_2)\right)\right\}\right]. \qquad [9]$$

Dependence of the electric field strength at a distance r [km] from the transmitter, taking into account the transmitting antenna gain G_1 and the transmitter power P_1 [kW] (Equation 10).

$$A = \frac{173 \cdot \sqrt{P_1 \cdot G_1}}{r}, \text{[mV/m]}. \qquad [10]$$

The results of modeling Equations 8 to 10 in the MathLab environment are shown in Figures 3(a) and 3(b). The reflection coefficient's dependences on the incidence angle for vertical and horizontal polarization used in the simulation correspond to Figure 1(a).
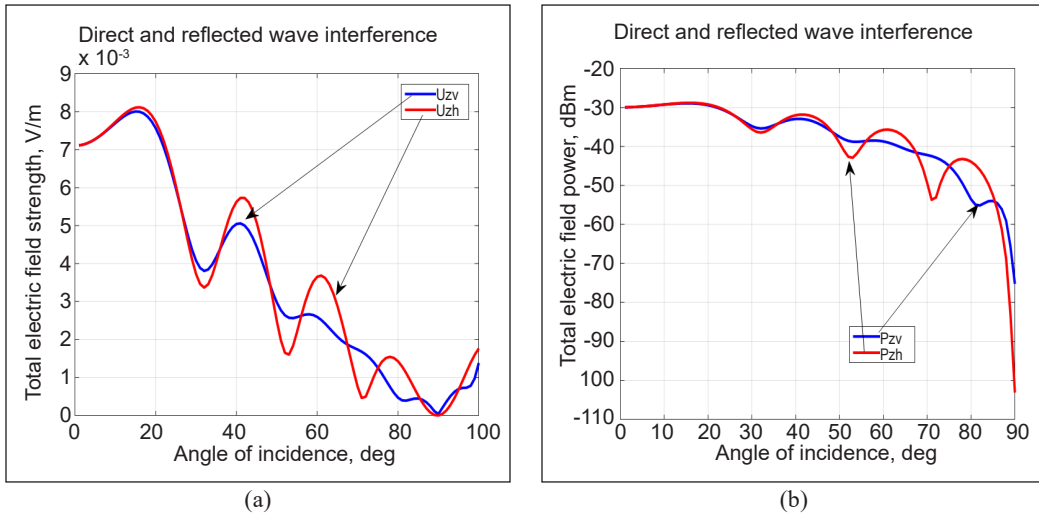
(a)   (b)

Figure 3. The results of modeling the interference of the incident and reflected waves: (a) field strength, V/m; (b) total electric field power, dBm

Analysis of the simulation results presented in Figure 3 allows drawing the following conclusions:

- The condition of total refraction (Brewster's effect) is accompanied by a change in the nature of the oscillations: at an angle of the incident (and reflected) signal smaller than Brewster's angle, the horizontally and vertically polarized waves arriving at the receiver are in-phase, and at a larger angle, a phase shift is observed between them;

- the level of the signal that enters the receiver at an angle of the incident (and reflected) signal greater than Brewster's angle, and represents the result of the passage of an electromagnetic wave below the air-surface interface, is sufficient for subsequent processing and analysis of the soil physical and chemical parameters;

- comparison of the oscillations of the total signal on vertical and horizontal polarization can serve as the basis for the algorithm of the joint flight of two UAVs that make up a bistatic radar system for remote soil sensing, which ensures the manifestation of the total refraction effect.

Figure 4 shows the conditions for implementing the flight algorithm (Figure 5) in determining Brewster's angle. Initial position: UAVs are at the same height at a distance of d_0, which ensures safe piloting
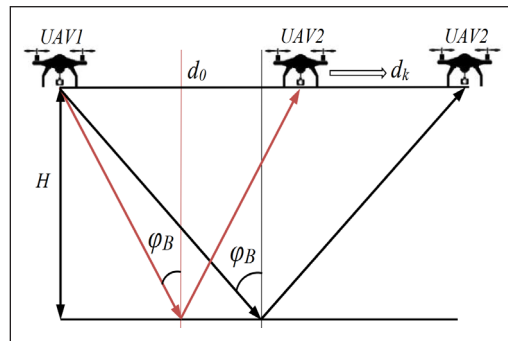

Figure 4. The UAVs' position while determining Brewster's angle

and the lowest possible value of Brewster's angle. The radio transmitter on the UAV1 irradiates the earth's surface with a radar signal with alternating horizontal and vertical polarization. The radio receiver located on the UAV2 receives the signal reflected from the earth's surface and fixes the level of the total reflected signal, changing the type of polarization of the received signal synchronously with the transmitting position.

UAV2 starts horizontal movement in the selected direction with zero roll and pitch angles. As UAV2 moves away from UAV1, the angle of incidence increases. The change in the level of the reflected signal is recorded in the radio receiver, and sequences of measured values of interference wave oscillations are formed in each polarization variant. The angle at which the oscillations of a vertically polarized wave shift in phase relative to the oscillations of a horizontally polarized wave is fixed as the required Brewster's angle. All algorithm steps (Figure 5) can be repeated to increase the reliability of the result.
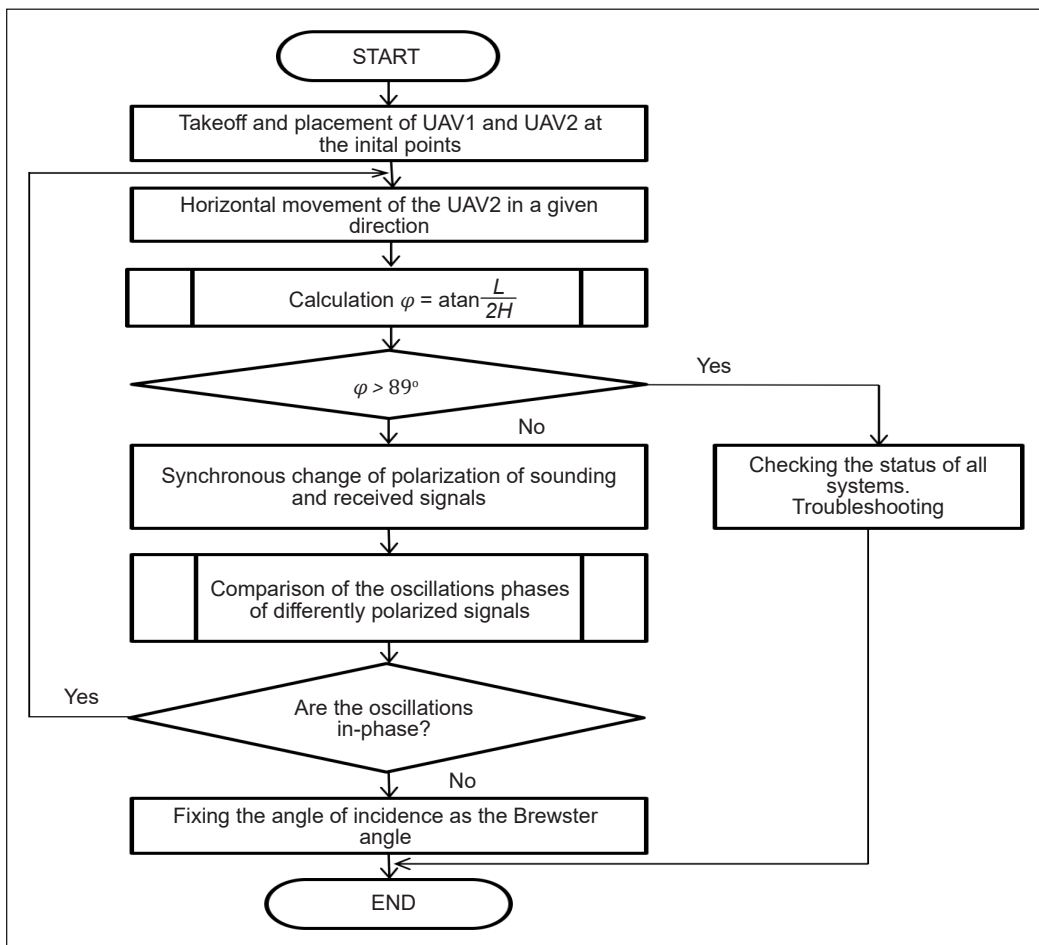

Figure 5. Algorithm for the joint flight of the two UAVs' bistatic radar system for remote soil sensing, which ensures the detection of the effect of total refraction

The termination condition of the algorithm is the opposite of the condition for the applicability of the Vvedensky formula presented in Equation 11 when the effect of interference of the direct and reflected waves can be neglected:

$$L < \frac{18 \cdot h_1 \cdot h_2}{\lambda}.$$ [11]

The implementation of the proposed algorithm puts forward requirements for the implementational accuracy of the following tasks:
- the implementation of a horizontal flight of a UAV with a receiver in a given direction;
- stationary hovering of a UAV with a transmitter at the same height as the moving UAV;
- determining the distance between UAVs;
- determination of the distance from each UAV to the place of radio signal reflection from the earth's surface;
- determination of the flight altitude of each UAV.

Both UAVs have GPS/GLONASS navigation systems to solve the navigation task. Typically, the GPS signal accuracy of satellite navigation systems in horizontal dimensions is approximately 1–2 meters (assuming good sky visibility). Altitude accuracy (over the sea) is usually 2–5 times less than positioning accuracy under the same conditions (i.e., from 2 to 10 meters under perfect conditions). Since the distance between UAVs is less than 100 meters, the reason for positioning errors for both UAVs will be the same, and errors will be compensated while determining their relative position.

The required accuracy of calculating the angular values is 1 degree, which is ensured even with positioning errors of 2–3 meters.

Analysis of the mathematical equations required for algorithm implementation showed that the computational complexity for these algorithms is low and can be implemented by an on-board RISC microcontroller with a clock frequency of 120 Mhz and a memory capacity of 128 KB, in addition to the execution of existing flight control algorithms.

RESULTS AND DISCUSSION

Experimental studies were conducted to validate the efficiency of the proposed algorithm.

Experimental design includes:
- a transmitting Yagi antenna, permanently located at the height of 5.6 m, designed for the decimeter range of the television signal;
- a spike antenna placed on a freely movable base at the height of 1.2 m;
- a Kenwood TK-450S transmitter tuned to a 469 MHz frequency, free from other radio transmitting devices operating in the experiment area;

- the analyzer of radio engineering paths and signals, portable S362E from Anritsu Company;
- TDR 150 moisture meter to measure humidity and conductivity at the radio signal reflection spot;
- a transmitting antenna turntable that allows setting the incidence angle in increments of 5 degrees.

The vegetation and surface relief at the test site ensured the Raleigh requirement to implement specular reflection. The soil dispersion under the entire experiment conditions remained unchanged. The general scheme of the experiment was similar to the scheme shown in Figure 2. Equation 11 was provided for the range of spatial relationships of the UAVs.

A series of two experiments were conducted. During the first experiment, the measured specific conductivity was σ=0.017 S/m, soil moisture vwc= 19.9%, Brewster's angle calculated value φ_B =66°C, and the reflection coefficient R_V=0.023. The results of the experiment are presented in Figure 6(a).

During the second experiment, the specific conductivity was σ=0.06 S/m, soil moisture vwc=34%, the calculated value of Brewster's angle φ_B= 67°C, and the reflection coefficient value R_V=0.089. The results of the experiment are shown in Figure 6(b).

The results of experimental studies show that at an angle of incidence greater than the value of Brewster's angle, a phase shift is formed between the oscillations of interference waves with vertical and horizontal polarizations. At higher humidity, an increase in the reflection coefficient is observed, resulting in a significant increase in the amplitude of the interference waves. An increase in soil conductivity by a factor of 3.5 (from 0.017 to 0.06 cm/m) provided an increase in Brewster's angle by only one degree, but at the same time, the minimum value of the reflection coefficient increased from 0.023 to 0.089. The
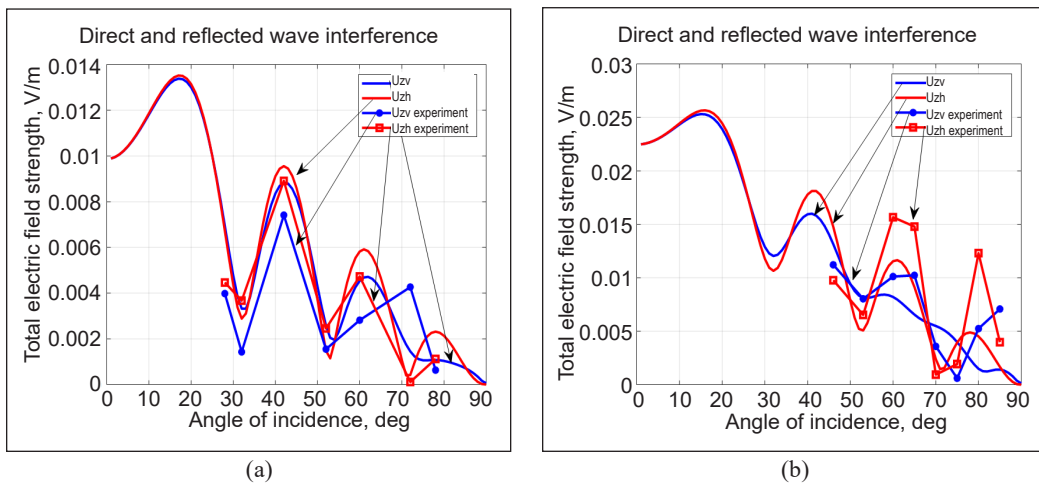

Figure 6. Results of the experiment: (a) soil specific conductivity 0.017 S/m, soil moisture 19.9%; (b) soil specific conductivity 0.06 S/m, soil moisture 34%

experimental data are in good agreement with the simulation results. At the extremum points, the relative arrangement of the amplitudes of the interference waves of horizontal and vertical polarization obtained experimentally and by the method of mathematical modeling coincides. Some deviations of the experimental data from the calculated ones may be due to the representation of the relief when modeling a smooth surface, and in the experiment, there was vegetation and minor irregularities (with the Rayleigh constraints for specular reflection). Mathematical modeling and experimental studies confirmed the possibility of using the emerging phase shift in the oscillations of interference waves with horizontal and vertical polarization as a sign of transition through the incidence angle with the effect of total refraction. The level of the reflected signal at vertical polarization is formed considering the physicochemical parameters of the soil subsurface layers. A proportional increase in the signal level is observed with an increase in soil conductivity due to an increase in its moisture.

The obtained experimentally confirmed method of measuring Brewster's angle by comparing the oscillations of horizontally and vertically polarized interference waves makes it possible, under conditions of a priori uncertainty in the soil physical and chemical parameters, to create conditions for subsurface radar sounding.

Determination of Brewster's angle allows calculating the dielectric constant of topsoil and estimating the moisture percentage by its change over a certain observation period.

Using "skew" irradiation of soil at an incidence angle close to Brewster's angle creates conditions for spreading the refracted radio signal in a depth of several meters and can be used for determining the groundwater level and estimating the moisture percentage accumulated during the autumn-winter period. Based on this information, reasonable agricultural decisions can be made for efficient crop production.

The next steps in creating a georadar based on a bistatic system of two UAVs are the justification of the receiving and transmitting antennas' designs, the choice of the probing signal's modulation type, and the formation of requirements for the controller of the receiving equipment. The authors associate the most likely direction in receiving equipment with SDR technology.

CONCLUSION

An algorithm for the joint flight of two crewless aerial vehicles that make up a bistatic radar system for remote sensing of the soil is proposed. Under conditions of absence regarding the soil's physical and chemical parameters, this algorithm makes it possible to determine Brewster's angle at which the subsurface soil layers contribute to the reflected signal.

The proposed algorithm provides conditions under which the reflection from the air-soil interface is minimized and allows for solving various problems: to assess soil moisture in the root zone, determine the groundwater level and find extensive inhomogeneities.

Gennady Linets, Anatoliy Bazhenov, Sergey Malygin, Natalia Grivennaya, Tatiana Chernysheva and Sergey Melnikov

The level of oscillations of interferential waves and their mutual phase shift can serve as information markers for assessing the soil's physical and chemical parameters below the air-soil boundary, including moisture.

ACKNOWLEDGMENT

REFERENCES

Amazirh, A., Merlin, O., Er-Raki, S., Gao, Q., Rivalland, V., Malbeteau, Y., Khabba, S., & Escorihuela, M. J. (2018). Retrieving surface soil moisture at high spatio-temporal resolution from a synergy between Sentinel-1 radar and Landsat thermal data: A study case over bare soil. *Remote Sensing of Environment*, *211*, 321-337. https://doi.org/10.1016/j.rse.2018.04.013

Babaeian, E., Paheding, S., Siddique, N., Devabhaktuni, V. K., & Tuller, M. (2021). Estimation of root zone soil moisture from ground and remotely sensed soil information with multisensor data fusion and automated machine learning. *Remote Sensing of Environment*, *260*, Article 112434. https://doi.org/10.1016/j.rse.2021.112434

Bandini, F., Sunding, T. P., Linde, J., Smith, O., Jensen, I. K., Köppl, C. J., Butts, M., & Bauer-Gottwein, P. (2020). Unmanned Aerial System (UAS) observations of water surface elevation in a small stream: Comparison of radar altimetry, LIDAR and photogrammetry techniques. *Remote Sensing of Environment*, *237*, Article 111487. https://doi.org/10.1016/j.rse.2019.111487

Barca, E., De Benedetto, D., & Stellacci, A. M. (2019). Contribution of EMI and GPR proximal sensing data in soil water content assessment by using linear mixed effects models and geostatistical approaches. *Geoderma*, *343*, 280-293. https://doi.org/10.1016/j.geoderma.2019.01.030

Bargiel, D., Herrmann, S., & Jadczyszyn, J. (2013). Using high-resolution radar images to determine vegetation cover for soil erosion assessments. *Journal of Environmental Management*, *124,* 82-90. https://doi.org/10.1016/j.jenvman.2013.03.049

Bazhenov, A., Sagdeev, K., Goncharov, D., & Grivennaya, N. (2021). Bistatic system for radar sensing of soil moisture. *International Scientific Conference Engineering for Rural Development (ERDev)*, *Jelgava, Latvia, 2021*, 919-925. https://doi.org/10.22616/ERDev.2021.20.TF207

Bhogapurapu, N., Dey, S., Homayouni, S., Bhattacharya, A., & Rao, Y.S. (2022). Field-scale soil moisture estimation using sentinel-1 GRD SAR data. *Advances in Space Research*, *70*(12), 3845-3858. https://doi.org/10.1016/j.asr.2022.03.019

Brook, A., De Micco, V., Battipaglia, G., Erbaggio, A., Ludeno, G., Catapano, I., & Bonfante, A. (2020). A smart multiple spatial and temporal resolution system to support precision agriculture from satellite images: Proof of concept on Aglianico vineyard. *Remote Sensing of Environment*, *240*, Article 111679, https://doi.org/10.1016/j.rse.2020.111679

Chandra, M., & Tanzi, T. J. (2018). Drone-borne GPR design: Propagation issues. *Comptes Rendus Physique*, *19*(1-2), 72-84. https://doi.org/10.1016/j.crhy.2018.01.002

Dari, J., Quintana-Seguí, P., Escorihuela, M. J., Stefan, V., Brocca, L., & Morbidelli, R., (2021). Detecting and mapping irrigated areas in a Mediterranean environment by using remote sensing soil moisture and a land surface model. *Journal of Hydrology*, *596*, Article 126129. https://doi.org/10.1016/j.jhydrol.2021.126129

Elkharrouba, E., Sekertekin, A., Fathi, J., Tounsi, Y., Bioud, H., & Nassim, A. (2022). Surface soil moisture estimation using dual-Polarimetric Stokes parameters and backscattering coefficient. *Remote Sensing Applications: Society and Environment*, *26*, Article 100737. https://doi.org/10.1016/j.rsase.2022.100737

Faye, G., Frison, P. L., Diouf, A. A., Wade, S., Kane, C. A., Fussi, F., Jarlan, L., Niang, M. F. K., Ndione, J. A., Rudant, J. P., & Mougin, E. (2018). Soil moisture estimation in Ferlo region (Senegal) using radar (ENVISAT/ASAR) and optical (SPOT/VEGETATION) data. *The Egyptian Journal of Remote Sensing and Space Science*, *21*(Supplement 1), 13-22. https://doi.org/10.1016/j.ejrs.2017.11.005

Filion, R., Bernier, M., Paniconi, C., Chokmani, K., Melis, M., Soddu, A., Talazac, M., & Lafortune, F.-X. (2016). Remote sensing for mapping soil moisture and drainage potential in semi-arid regions: Applications to the Campidano plain of Sardinia, Italy. *Science of the Total Environment, 543*(Part B), 862-876. https://doi.org/10.1016/j.scitotenv.2015.07.068

Fugazza, D. G., Aletti, Bertoni, D., & Cavicchioli, D. (2022). Farmland use data and remote sensing for ex-post assessment of CAP environmental performances: An application to soil quality dynamics in Lombardy, *Remote Sensing Applications: Society and Environment*, *26*, Article 100723. https://doi.org/10.1016/j.rsase.2022.100723

Gago, J., Douthe, C., Coopman, R.E., Gallego, P.P., Ribas-Carbo, M., Flexas, J., Escalona, J., & Medrano, H. (2015). UAVs challenge to assess water stress for sustainable agriculture. *Agricultural Water Management*, *153*, 9-19. https://doi.org/10.1016/j.agwat.2015.01.020

Gopaiah, M., Saha, R., Das, I. C., Sankar, G. J., & Kumar, K. V. (2021). Quantitative assessment of aquifer potential in near shore coastal region using geospatial techniques and ground penetrating radar, *Estuarine, Coastal and Shelf Science*, *262*, Article 107590. https://doi.org/10.1016/j.ecss.2021.107590

Ivushkin, K., Bartholomeus, H., Bregt, A. K., Pulatov, A., Franceschini, M. H. D., Kramer, H., van Loo, E. N., Jaramillo Roman, V. J., & Finkers, R. (2019). UAV based soil salinity assessment of cropland. *Geoderma, 338*, 502-512. https://doi.org/10.1016/j.geoderma.2018.09.046

Kaasiku, T., Praks, J., Jakobson, K., & Rannap, R. (2021). Radar remote sensing as a novel tool to assess the performance of an agri-environment scheme in coastal grasslands. *Basic and Applied Ecology*, *56*, 464-475. https://doi.org/10.1016/j.baae.2021.07.002

Kim, J. Y. (2021). Software design for image mapping and analytics for high throughput phenotyping. *Computers and Electronics in Agriculture*, *191*, Article 106550. https://doi.org/10.1016/j.compag.2021.106550

Li, Z. L., Leng, P., Zhou, C., Chen, K. S., Zhou, F. C. & Shang, G. F. (2021). Soil moisture retrieval from remote sensing measurements: Current knowledge and directions for the future. *Earth-Science Reviews*, *218*, Article 103673. https://doi.org/10.1016/j.earscirev.2021.103673

Ludeno, G., Catapano, I., Renga, A., Vetrella, A.R., Fasano, G., & Soldovieri, F. (2018). Assessment of a micro-UAV system for microwave tomography radar imaging. *Remote Sensing of Environment*, *212*, 90-102. https://doi.org/10.1016/j.rse.2018.04.040

Mallet, F., Marc, V., Douvinet, J., Rossello, P., Joly, D., & Ruy, S. (2020). Assessing soil water content variation in a small mountainous catchment over different time scales and land covers using geographical variables. *Journal of Hydrology*, *591*, Article 125593. https://doi.org/10.1016/j.jhydrol.2020.125593

Mandal, D., Kumar, V., Ratha, D., Dey, S., Bhattacharya, A., Lopez-Sanchez, J. M., McNairn, H., & Rao, Y. S. (2020). Dual polarimetric radar vegetation index for crop growth monitoring using sentinel-1 SAR data. *Remote Sensing of Environment*, *247*, Article 111954. https://doi.org/10.1016/j.rse.2020.111954

Martins, R. N., Portes, M. F., Fialho e Moraes, H. M., F. Junior, M. R., Fim Rosas, J. T., & Orlando Junior, W. A. (2021). Influence of tillage systems on soil physical properties, spectral response and yield of the bean crop. *Remote Sensing Applications: Society and Environment*, *22*, Article 100517, https://doi.org/10.1016/j.rsase.2021.100517

Nguyen, T. T., Ngo, H. H., Guo, W., Chang, S. W., Nguyen, D. D., Nguyen, C. T., Zhang, J., Liang, S., Bui, X. T., & Hoang, N. B. (2022). A low-cost approach for soil moisture prediction using multi-sensor data and machine learning algorithm. *Science of the Total Environment*, *833*, Article 155066. https://doi.org/10.1016/j.scitotenv.2022.155066

Pandey, A., & Jain, K. (2022) An intelligent system for crop identification and classification from UAV images using conjugated dense convolutional neural network. *Computers and Electronics in Agriculture*, *192*, Article 106543.https://doi.org/10.1016/j.compag.2021.106543

Rohil, M. K., & Mathur, S. (2022). CYGNSS-derived soil moisture: Status, challenges and future. *Ecological Informatics*, *69*, Article 101621. https://doi.org/10.1016/j.ecoinf.2022.101621

Rouf, T., Girotto, M., Houser, P., & Maggioni, V. (2021) Assimilating satellite-based soil moisture observations in a land surface model: The effect of spatial resolution. *Journal of Hydrology*, *13*, Article 100105. https://doi.org/10.1016/j.hydroa.2021.100105

Saddik, A., Latif, R., Elhoseny, M., & El Ouardi, A. (2021). Real-time evaluation of different indexes in precision agriculture using a heterogeneous embedded system. *Sustainable Computing: Informatics and Systems*, *30*, Article 100506. https://doi.org/10.1016/j.suscom.2020.100506

Sahaar, S. A., Niemann, J. D., & Elhaddad, A. (2022). Using regional characteristics to improve uncalibrated estimation of rootzone soil moisture from optical/thermal remote-sensing. *Remote Sensing of Environment*, *273*, Article 112982. https://doi.org/10.1016/j.rse.2022.112982

Salam, A., Vuran, M.C., & Irmak, S. (2019). Di-Sense: In situ real-time permittivity estimation and soil moisture sensing using wireless underground communications. *Computer Networks*, *151*, 31-41. https://doi.org/10.1016/j.comnet.2019.01.001

Su, C. H., Ryu, D., Crow, W. T., & Western, A. W. (2014). Stand-alone error characterisation of microwave satellite soil moisture using a Fourier method. *Remote Sensing of Environment*, *154*, 115-126. https://doi.org/10.1016/j.rse.2014.08.014

Tavakol, A., McDonough, K. R., Rahmani, V., Hutchinson, S. L., & Hutchinson, J. M. S. (2021). The soil moisture data bank: The ground-based, model-based, and satellite-based soil moisture data.

Remote Sensing Applications: Society and Environment, *24*, Article 100649. https://doi.org/10.1016/j.rsase.2021.100649

Tran, A. P., Bogaert, P., Wiaux, F., Vanclooster, M., & Lambot, S. (2015). High-resolution space–time quantification of soil moisture along a hillslope using joint analysis of ground penetrating radar and frequency domain reflectometry data. *Journal of Hydrology*, *523*, 252-261. https://doi.org/10.1016/j.jhydrol.2015.01.065

Wang, H., Magagi, R., Goïta, K., Colliander, A., Jackson, T., McNairn, H., & Powers, J. (2021). Soil moisture retrieval over a site of intensive agricultural production using airborne radiometer data. *International Journal of Applied Earth Observation and Geoinformation*, *97*, Article 102287. https://doi.org/10.1016/j.jag.2020.102287

Wang, S., Zhang, K., Chao, L., Li, D., Tian, X., Bao, H., Chen, G., & Xia, Y. (2021). Exploring the utility of radar and satellite-sensed precipitation and their dynamic bias correction for integrated prediction of flood and landslide hazards. *Journal of Hydrology*, *603*, Article 126964, https://doi.org/10.1016/j.jhydrol.2021.126964

Xie, F., Lai, W.W. L., & Dérobert, X. (2022). Building simplified uncertainty models of object depth measurement by ground penetrating radar. *Tunnelling and Underground Space Technology*, *123*, Article 104402. https://doi.org/10.1016/j.tust.2022.104402

Yang, H., Xiong, L., Liu, D., Cheng, L., & Chen, J. (2021). High spatial resolution simulation of profile soil moisture by assimilating multi-source remote-sensed information into a distributed hydrological model. *Journal of Hydrology*, *597*, Article 126311. https://doi.org/10.1016/j.jhydrol.2021.126311

Zhu, L., Walker, J. P., Tsang, L., Huang, H., Ye, N., & Rüdiger, C. (2019). Soil moisture retrieval from time series multi-angular radar data using a dry down constraint. *Remote Sensing of Environment*, *231*, Article 111237. https://doi.org/10.1016/j.rse.2019.111237